JBC RESEARCH ARTICLE

Small molecule LATS kinase inhibitors block the Hippo signaling pathway and promote cell growth under 3D culture conditions

Received for publication, December 2, 2021, and in revised form, February 21, 2022 Published, Papers in Press, February 26, 2022,
https://doi.org/10.1016/j.jbc.2022.101779

Ayako Aihara[1], **Takumi Iwawaki**[1], **Natsuki Abe-Fukasawa**[1], **Keiichiro Otsuka**[2], **Koichiro Saruhashi**[2], **Takumi Mikashima**[2], **and Taito Nishino**[1,*]

From the [1]*Biological Research Laboratories, Nissan Chemical Corporation, Saitama, Japan;* [2]*Head office, Nissan Chemical Corporation, Tokyo, Japan*

Edited by Henrik Dohlman

Although 3D cell culture models are considered to reflect the physiological microenvironment and exhibit high concordance with *in vivo* conditions, one disadvantage has been that cell proliferation is slower in 3D culture as compared to 2D culture. However, the signaling differences that lead to this slower proliferation are unclear. Here, we conducted a cell-based high-throughput screening study and identified novel small molecules that promote cell proliferation, particularly under 3D conditions. We found that one of these molecules, designated GA-017, increases the number and size of spheroids of various cell-types in both scaffold-based and scaffold-independent cultures. In addition, GA-017 also enhances the *ex vivo* formation of mouse intestinal organoids. Importantly, we demonstrate that GA-017 inhibits the serine/threonine protein kinases large tumor suppressor kinase 1/2, which phosphorylate Yes-associated protein and transcriptional coactivator with PDZ-binding motif , key effectors of the growth- and proliferation-regulating Hippo signaling pathway. We showed that GA-017 facilitates the growth of spheroids and organoids by stabilizing and translocating Yes-associated protein and transcriptional coactivator with PDZ-binding motif into the cell nucleus. Another chemical analog of GA-017 obtained in this screening also exhibited similar activities and functions. We conclude that experiments with these small molecule large tumor suppressor kinase inhibitors will contribute to further development of efficient 3D culture systems for the *ex vivo* expansion of spheroids and organoids.

To investigate cellular functions and behaviors *in vitro*, 2D cell culture models have become the established standard method of practice. 2D culture methods have fulfilled a crucial role for elucidating various cellular activities, including proliferation, self-renewal of stem cells, and their differentiation (1). However, many 2D culture methods involve attachment of a cell monolayer to the flat and hard surface of artificial plastic substrates, which are quite different from the *in vivo* extracellular matrix (ECM) microenvironment in tissues and organs. Even if ECM factors are used to coat the surface of a cell culture vessel, adhering cells recognize the stiffness of the substrate as a factitious environment (2). The cells cultured under 2D conditions completely differ from *in vivo* status where cells grow under 3D conditions. Therefore, 2D cell monolayer cultures are unlikely to accurately reflect the physiological conditions of *in vivo* tissues and organs.

Various 3D cell culture methods have recently been developed to address the aforementioned drawbacks of 2D culture. These methods allow cells to form aggregates (spheroids) *via* the use of scaffolds such as gel matrices and micro-carriers, liquid culture in low-attachment plates, or hanging drops (3, 4). Spheroids formed in 3D cell culture systems undergo cell–cell interactions from all angles and also exhibit cell-ECM interactions (5). These interactions likely mimic the *in vivo* cellular microenvironment and behavior and reflect *in vivo* physiological conditions better than 2D cultures. In particular, the drug sensitivity of 3D tumor spheroids was shown to be more clinically relevant in anticancer drug screening than that of 2D monolayer cells (6). Based on these findings, we have developed 3D cell culture systems suitable for high throughput screening (HTS) (7).

Recently developed organoid cultures also employ 3D culture methods coupled with ECM hydrogels (*e.g.*, Matrigel) to analyze organ behavior and function *ex vivo* (8, 9). Organoid culture methods have been developed to study a wide range of organs, including the intestines, kidney, liver, brain, stomach, lung, and pancreas (10). Moreover, organoids have made a significant impact on stem cell and developmental biology and have become a useful tool for drug screening. As such, the development of 3D culture methods for spheroid and organoid formation has attracted considerable attention over the last 10 years. However, most cells in spheroids and organoids grow slowly compared to those in 2D cultures (11), which lead to difficulties in producing them readily and cost-effectively. This is especially crucial with respect to spheroid/organoid-based HTS that utilizes limited cellular resources in drug discovery. Consequently, more efficient culture methods for *ex vivo* spheroid/organoid expansion need to be identified.

In this study, we explored small molecules that would promote cell proliferation, especially under 3D conditions,

* For correspondence: Taito Nishino, nishino@nissanchem.co.jp.

© 2022 THE AUTHORS. Published by Elsevier Inc on behalf of American Society for Biochemistry and Molecular Biology. This is an open access article under the CC BY-NC-ND license (http://creativecommons.org/licenses/by-nc-nd/4.0/).

applying an in-house chemical library for target screening. To this end, we employed a 3D culture method that leverages a polysaccharide, gellan gum (7), to implement efficient cell-based HTS. As a result of the screening, we identified several small molecules with targeted activities, one of which was designated GA-017. We found that GA-017 enhanced the formation of spheroids and organoids under multiple 3D conditions. Moreover, transcriptome and immunocytochemistry analyses revealed that GA-017 inhibited the phosphorylation of Yes-associated protein and transcriptional coactivator with PDZ-binding motif (YAP/TAZ) (12, 13) and promoted their nuclear translocation. This in turn led to the induction of downstream cell growth–promoting genes. Finally, we demonstrated that GA-017 inhibited the activity of large tumor suppressor kinase 1 and 2 (LATS1/2) (14), components of the Hippo pathway (15, 16) that mediate phosphorylation of YAP/TAZ. Our results offer a novel 3D cell culture method using GA-017 that can serve as a more efficient and practical system for *ex vivo* expansion of spheroids/organoids.

Results

Identification of small molecules that enhance cell growth in 3D cultures by cell-based HTS

We assumed that some small molecule compounds preferentially activate signals that facilitate the growth of cells under 3D conditions. For this reason, we first established an efficient HTS system to detect the proliferation of cells under anchorage-independent conditions (Fig. 1*A*), utilizing gellan gum to suspend cell spheroids homogeneously on low-attachment plates (7). The addition of gellan gum to medium is an effective way to prevent the formation of large-sized spheroids and increase sensitivity to test compounds (7). We employed SKOV3 ovary cancer cells as the target for screening because of their robust spheroid-forming ability in gellan gum–containing medium, in addition to their clear sensitivity to external stimuli such as growth factors under 3D culture conditions (7). In this HTS system, the coefficient of variation and Z′-factor for 384-well plates when counting the number of SKOV3 cells using a water-soluble tetrazolium salt WST-8 were 5.76 ± 1.77 and 0.74 ± 0.07, respectively. We next screened a library of over 50,000 chemically synthesized compounds for activity in promoting the proliferation of suspended SKOV3 cells. As a result, a total of nine of the preliminary hit compounds increased the number of cells by more than 1.5 times (Table S1). Furthermore, we performed structure-activity optimization of the hit compounds, focusing attention on one of the most active compounds, which we designated GA-017 (Fig. 1*B*).

GA-017 increased the number of SKOV3 cells in anchorage-independent cultures containing gellan gum more efficiently than the vehicle control (dimethyl sulfoxide, DMSO), whereas GA-017 did not affect cell growth under 2D conditions (Fig. 1, *C–E*). While SKOV3 cells cultured in the control medium presented compacted spheroids, those grown with GA-017 presented grape-like morphology, in which loosely attached individual cells were identifiable (Fig. 1*C*). We also confirmed the positive effect of GA-017 on cell proliferation by directly counting the number of individual cells within each spheroid (Fig. S1*A*). Dose-response experiments revealed that GA-017 facilitated SKOV3 cell growth with a half-maximal effective concentration (EC_{50}) of 3.51 ± 0.26 μM (Fig. 1*F*). At the maximally effective concentration, 10 μM, GA-017 increased the number of SKOV3 cells over 2-fold. Furthermore, GA-017 significantly enhanced the growth of a variety of animal cells including human, murine, hamster, monkey, and canine cell types, except for HepG2 and LNCap cells, which are likely independent of their origin or source (Table S2). In particular, GA-017 markedly enhanced the growth of human umbilical vein endothelial cells (HUVECs) under anchorage-independent conditions (Table S2).

GA-017 expands spheroids and organoids under various 3D cell culture conditions

We examined the effect of GA-017 on cell proliferation under 3D conditions that are more commonly employed to prepare spheroids and organoids, that is, the use of 3D cultures in round-bottom (U-bottom) wells of low-attachment culture plates and in hanging drops. GA-017 increased both spheroid size and the number of SKOV3 cells, when cultured up to 6 days in U-bottom wells of low-attachment culture plates (Fig. 2, *A* and *B*). Furthermore, an increase was observed in multiple types of cells (Table S3). Among the tested cell types, GA-017 augmented the growth of HUVECs most effectively (Table S3). Fig. S1*B* shows that HUVECs lost their viability on day 4 under 3D conditions, and GA-017 suppressed the cell death of HUVECs and promoted their cell growth. On the other hands, SKOV3 cells did not lose their viability and grew mildly under 3D conditions (Fig. 2*B*). Therefore, the effects of GA-017 were relatively modest on cancer cell lines such as SKOV3 cells, while it was remarkable on HUVECs. HUVECs cultured with GA-017 expressed the endothelial markers *PECAM1* and *VWF* mRNA at levels equal to or greater than the vehicle control (Fig. S1*C*). HUVEC spheroids cultured with GA-017 consistently expressed PECAM1 and vWF proteins (Fig. S1*D*), suggesting that GA-017 promoted the growth of HUVEC spheroids while maintaining their cell function. GA-017 also promoted the growth of spheroids formed in hanging drops (Fig. 2, *C* and *D*).

Next, we tested whether GA-017 affects cyst or organoid formation in gel-embedded 3D cultures. To evaluate the effect of GA-017 on the formation of cysts, we employed Madin-Darby canine kidney (MDCK) cells, which are widely used as an *in vitro* model of epithelial cysts. We cultured MDCK cells in the presence of GA-017 in Matrigel for 6 days. MDCK cells formed cysts in both control (DMSO)- and GA-017–treated conditions, with actin cytoskeleton lining the lumen and β-catenin on the lateral cell membrane (Fig. 2*E*). There was no clear difference in apical-basal polarity between the two conditions. We also found that the number of cysts in cultures with GA-017 was 1.5-fold higher than the vehicle control (DMSO) (Fig. 2*F*). The proportion of large-sized cysts (>70 μm in diameter) was also increased in cultures with GA-017 as compared to the vehicle control (Fig. 2*G*). The

ASBMB

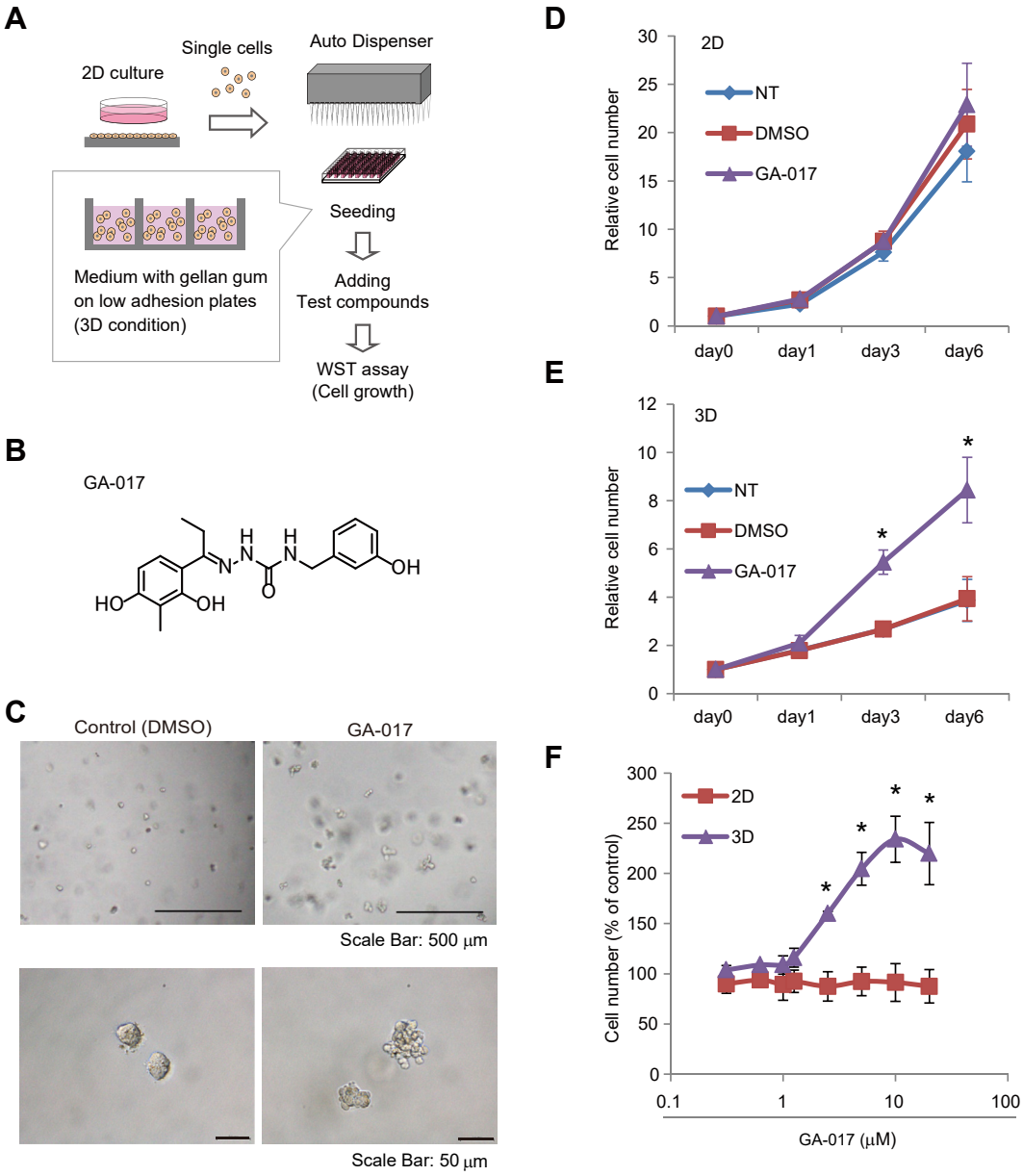

Figure 1. Identification of GA-017. *A*, illustration of high-throughput screening for cell growth regulators under 3D conditions using gellan gum. SKOV3 cells were suspended in medium containing gellan gum and dispersed in wells of low-attachment microplates. The cells formed spheroids during the culture while suspended. *B*, the chemical structure of GA-017. *C*, images of SKOV3 cells cultured in gellan gum–containing medium with DMSO or 10 μM GA-017 for 4 days. *Left*: control (DMSO), *right*: 10 μM GA-017, *upper*: low magnification, *lower*: high magnification. The bars represent 50 or 500 μm. *D* and *E*, time course of SKOV3 cell growth under 2D (*D*) or 3D (*E*) conditions evaluated using an ATP assay. The cell numbers on each day were normalized by the value on day 0. DMSO: vehicle control, GA-017: 10 μM GA-017. *F*, dose-dependent effect of GA-017 on SKOV3 cell growth evaluated using an ATP assay under 2D or 3D (with gellan gum) conditions for 4 days of culture. Y-axis indicates relative cell number (% of control) to vehicle control (DMSO). The data represent means ± SD of 3 to 4 independent experiments. Statistical significance was analyzed using Dunnett's test for *D*, *E*, and *F*. *$p<0.01$. DMSO, dimethyl sulfoxide; NT, nontreatment,.

results of Figure 2, *F* and *G* show that GA-017 not only increased the size of individual cysts but also enhanced the cyst formation starting from single cells. Thus, it is speculated that GA-017 enhances the cyst formation by promoting both initial cyst formation and cell proliferation. In addition, GA-017 significantly enhanced the *ex vivo* formation of intestinal organoids as compared with the vehicle control (Fig. 2,*H* and *I*). Intestinal organoids cultured with GA-017 showed similar morphology to those with DMSO, where the central lumen was surrounded by budding crypt-like domains (Fig. 2*H*). GA-017 increased the proportion of large-sized organoids (>300 μm in diameter) as compared to DMSO (Fig. 2*J*). Immunofluorescent analysis exhibited that intestinal organoids cultured with both DMSO and GA-017 contained cell types such as intestine cells (villin$^+$), enteroendocrine cells (CHGA$^+$), and paneth cells (Lysozyme$^+$) as shown in Fig. S2, *A*–*C*. Furthermore, there was no significant difference in the expression of the intestine marker villin1 (*Vil1*), the stem cell marker LGR5 (*Lgr5*), and the differentiation marker intestinal alkaline phosphatase (*Alpi*) between organoids cultured with

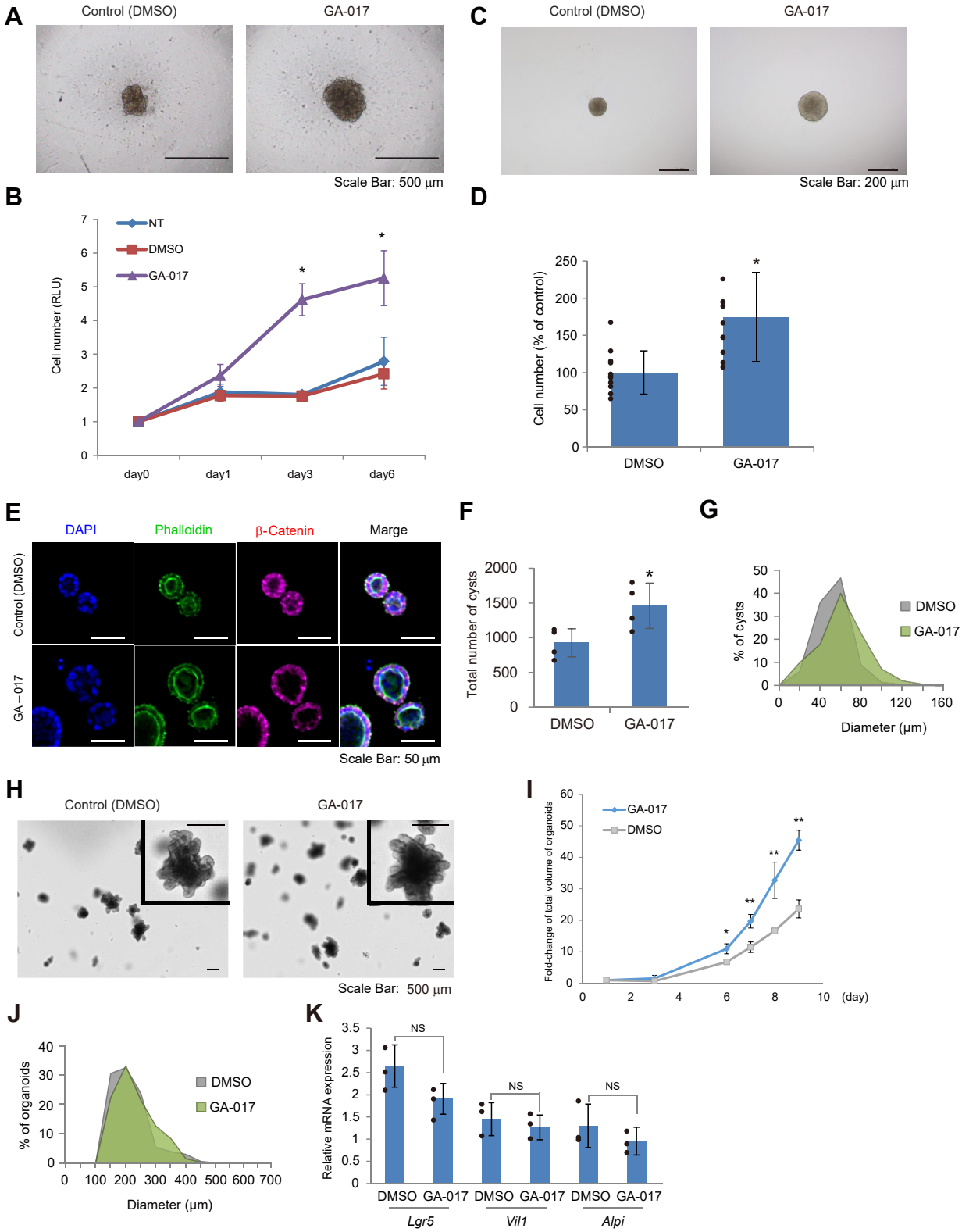

Figure 2. GA-017 promotes growth and/or organoid formation of SKOV3 and A431 spheroids, MDCK cysts, and mouse intestinal organoids. *A* and *B*, SKOV3 cells were cultured in wells of low-attachment U-bottom plates with DMSO or GA-017 for up to 6 days. *A*, images of SKOV3 cells cultured for 4 days in the well. *Left*: control (DMSO), *right*: 10 μM GA-017. The bars represent 500 μm. *B*, time course of SKOV3 cell growth evaluated using an ATP assay. Each RLU was normalized by that on day 0. DMSO: vehicle control, GA-017: 10 μM GA-017. The data represent means ± SD of three independent experiments. *$p<0.01$. *C* and *D*, A431 cells were cultured in hanging drops with DMSO or 10 μM of GA-017 for 2 days. *C*, images of A431 cells cultured in the drop. *Left*: control (DMSO), *right*: 10 μM GA-017. *D*, the number of cells cultured with DMSO or GA-017. Y-axis indicates relative cell number (% of control) to vehicle control (DMSO). The data represent means ± SD of 11 independent experiments. *$p<0.01$. *E* and *G*, MDCK cells were cultured in Matrigel for 6 days with DMSO (0.01%) or 10 μM GA-017. *E*, fluorescent images of MDCK cysts cultured for 6 days. *Upper*: control (DMSO), lower: 10 μM GA-017. β-catenin: *magenta*, phalloidin: *green*, nuclear (DAPI): *blue*. *F*, total number of MDCK cysts (diameter >30 μm). The data represent means ± SD of three independent experiments.

GA-017 and DMSO (Fig. 2*K*), suggesting that GA-017 promoted the expansion of intestinal organoids without affecting cell differentiation. Collectively, these results indicate that GA-017 is a specific small molecule with an ability to enhance the *ex vivo* formation of spheroids and organoids.

Next, we examined whether GA-017 is suitable for long-term 3D cultures. GA-017 increased the number of SKOV3 cells in gellan gum–containing 3D cultures more efficiently than the vehicle control (DMSO) over a period of 14 days (Fig. S1, *E* and *F*). Real-time quantitative PCR showed that SKOV3 cells cultured with GA-017 expressed the stem cell marker *POU5F1*, the migration marker *THBS*, and the invasion marker *MMP9* at the same level as cells cultured with DMSO (Fig. S1*G*). By contrast, expression of the epithelial-mesenchymal transition marker *SNAI1* was significantly decreased in cells cultured with GA-017 (Fig. S1*G*). SKOV3 cells cultured with GA-017 exhibited migration capability comparable to cells cultured with DMSO (Fig. S1*H*). Furthermore, GA-017 augmented the number of mesenchymal stem cells (MSCs) in gellan gum–containing 3D cultures over a period of 10 days, whereas MSCs did not grow in the presence of the vehicle control (DMSO) (Fig. S1*I*). GA-017 also increased the number of MSCs in 2D cultures as compared to DMSO, although the difference was not statistically significant (Fig. S1*I*). In both cultures, addition of GA-017 did not change the expression level of the MSC surface markers CD73 and CD90 (Fig. S1*J*). Real-time quantitative PCR showed that the expression of the stem cell marker *POU5F1*, the differentiation markers *PPARG* and *RUNX2*, and tumor-related genes *TP53*, *RB1*, *KRAS*, *SRC*, and *VEGFA* in MSCs cultured with GA-017 for 10 days was at the same level as on day 0 (Fig. S1*K*). In addition, GA-017 facilitated the expansion of intestinal organoids over a period of 21 days with two passages (Fig. S1*L*), suggesting the self-renewal capacity. Collectively, these results suggest that GA-017 exhibits growth-promoting effects even in long-term 3D cultures while maintaining the original cell function and stemness.

GA-017 promotes YAP/TAZ activation and nuclear translocation

We further investigated how GA-017 accelerates the growth of cells under 3D conditions. We first performed DNA microarray–mediated transcriptional profiling of SKOV3 cells cultured with GA-017 under 3D conditions and found greater up-regulation of Hippo pathway–regulated genes (*e.g.*, *ANKRD1*, *CYR61*, and *CTGF*) in GA-017–treated cells (Table S4). Gene ontology enrichment analysis revealed that regulation of Hippo signaling (GO term: 0035330) was enriched 19.6-fold ($p < 0.001$) in GA-017-treated cells (Table S5). GA-017 also altered the expression of Hippo signaling–related genes (Fig. 3*A*). These data suggest that GA-017 affects the expression of genes in the Hippo pathway, which reportedly plays an important role in organ size control, stem cell function, and tissue regeneration by governing cell growth and apoptosis (15, 16). We therefore hypothesized that GA-017 promotes cell proliferation by regulating the Hippo pathway. Real-time quantitative PCR analysis confirmed that GA-017 significantly induced the expression of the Hippo pathway–regulated genes *ANKRD1*, *CYR61*, and *CTGF* in SKOV3 cells in a time- and dose-dependent manner (Figs. 3, *B* and *C* and S3, *A–D*). Although these genes were up-regulated by GA-017 in both 2D and 3D cultures, the levels of increase were clearly higher in 3D compared to 2D cultures (Figs. 3, *B* and *C* and S3, *A–D*). These data indicate that GA-017 increases the expression of Hippo pathway–regulated genes more efficiently in cells under 3D *versus* 2D conditions, which may explain why GA-017 has little effect on cell proliferation in 2D cultures as shown in Figure 1*D*.

We next examined the effect of GA-017 on the activation state of YAP/TAZ (12, 13), known transcriptional co-activators in the Hippo pathway. Through Western blot analysis, we found that GA-017 inhibited the phosphorylation of YAP/TAZ in a dose-dependent manner under both 2D and 3D culture conditions and the inhibitory effect of GA-017 continued over 6 h (Fig. 3, *D* and *E* and Table S6). We also confirmed a GA-017 dose-dependent decrease in YAP phosphorylation using a quantitative assay involving homogeneous time-resolved fluorescence technology (Fig. S4, *A* and *B*). In other respects, GA-017 increased the levels of total TAZ protein under 3D conditions by time, and the repressed level of phosphorylated TAZ began to show some recovery by 6 h after the treatment (Fig. 3*E* and Table S6). We also observed that GA-017 increased the levels of phosphorylated LATS1/2 (14), core kinases for YAP/TAZ phosphorylation, over the indicated time course (Fig. 3, *D* and *E* and Table S6). Phosphorylation of LATS1/2 increases its kinase activity and subsequently phosphorylates YAP/TAZ (14). Mammalian Ste20-like kinase 1 (MST1) and MST2 phosphorylate and activate LATS1/2 (17). Real-time quantitative PCR showed that GA-017 significantly induced *LATS2* and MST1/2 (*STK3/4*) mRNA expression in SKOV3 cells (Fig. S3, *E* and *F*). Western blot analysis showed that GA-017 mildly increased the levels of total and phosphorylated MST1/2 protein while decreasing the level of LATS protein (Fig. S3*G* and Table S6). We additionally observed that GA-017 mildly increased the level of autophosphorylated LATS (Fig. S3*G* and Table S6). It has been reported that the Hippo pathway contains several levels of feedback systems (14, 18). One possible explanation of these data is GA-017–induced negative feedback loop that increased the MST1/2 expression, which subsequently increased phosphorylation of LATS1/2. However, despite the increase of LATS2 at the mRNA level, the total LATS protein level decreased over time

*$p<0.05$. *G*, size distribution of MDCK cysts formed in Matrigel with GA-017 or DMSO. Shown is the ratio to the total cyst number. *H–K*, mouse intestinal organoids were cultured in Matrigel for up to 9 days with DMSO (0.01%) or 10 μM GA-017. *H*, images of organoids cultured for 9 days in Matrigel. *Left*: control (DMSO), *right*: 10 μM GA-017. *I*, time course of organoid formation. Y-axis indicates the total volume of organoids/total volume of initial crypts (day 1). *$p<0.05$, **$p<0.01$. *J*, size distribution of intestinal organoids formed in Matrigel with GA-017 or DMSO. Shown is the ratio to the total organoid number. *K*, relative *Lgr5*, *Vil1*, and *Alpi* mRNA expression in organoids on day 9, normalized by *Gapdh*. The data represent means ± SD of three independent experiments. Statistical significance was analyzed using Dunnett's test for B or Student's *t* test for D, F, I, and K. *$p<0.01$. DMSO, dimethyl sulfoxide; MDCK, Madin-Darby canine kidney; NS, not significant; NT, nontreatment.

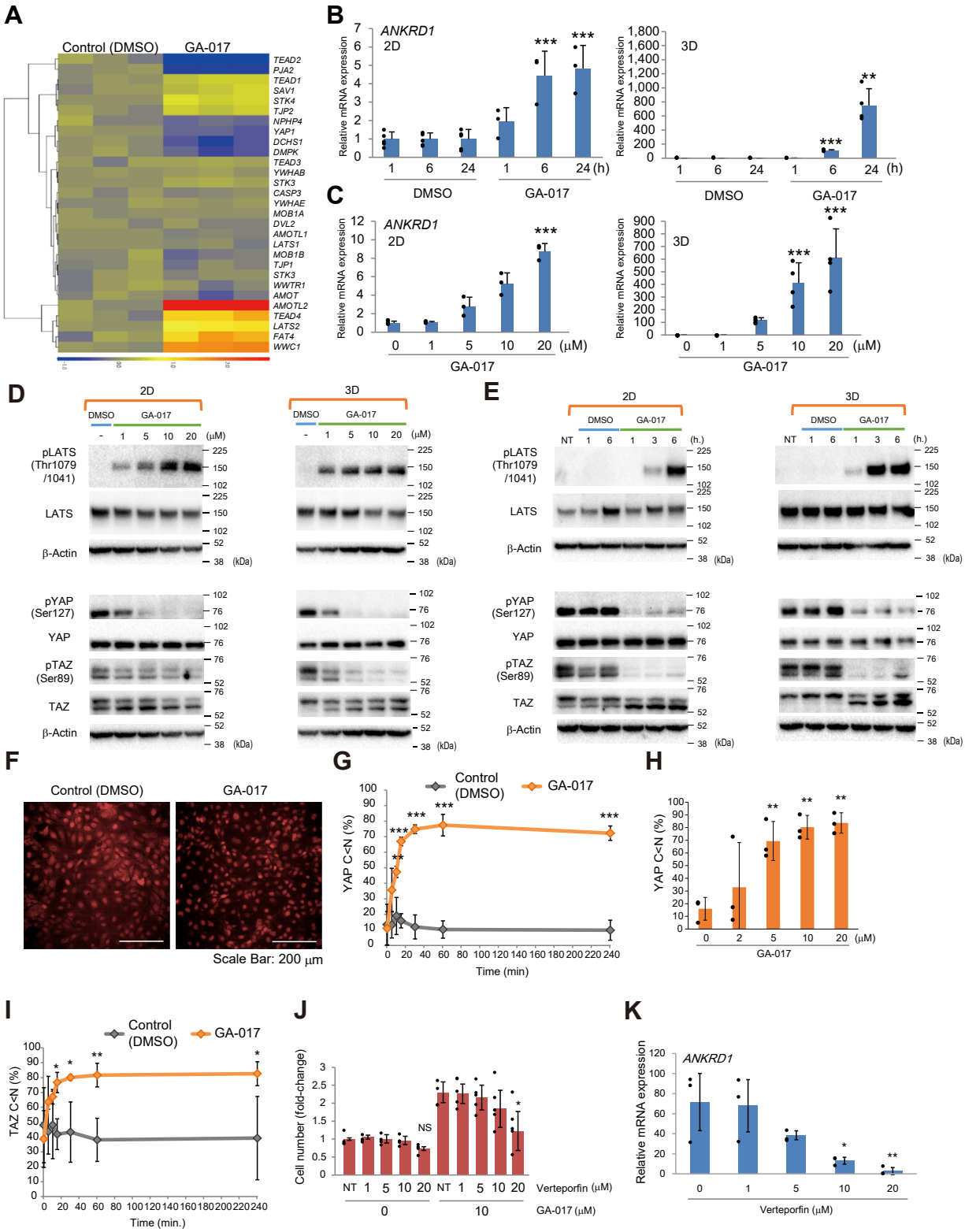

Figure 3. GA-017 promotes YAP nuclear translocation. *A*, heat map of Hippo signaling-related genes (GO:0035329) from DNA array data of SKOV3 cells cultured in gellan gum–containing medium with DMSO (control) or 10 μM GA-017 for 24 h. *B* and *C*, relative *ANKRD1* mRNA expression in SKOV3 cells cultured under 2D or 3D (with gellan gum) conditions with DMSO or GA-017. Signals were normalized by that of the *GAPDH* gene. Y-axis indicates relative mRNA expression to vehicle control (DMSO). Note the different scales of the Y-axes between 2D and 3D. The data represent means ± SD of three independent experiments. *B*, time course of *ANKRD1* expression in response to DMSO or 10 μM GA-017. *Left*: 2D, *right*: 3D. $^{**}p<0.01$, $^{***}p<0.001$. *C*, dose-response to GA-017 at 24 h. *Left*: 2D, *right*: 3D. $^{***}p<0.001$. *D* and *E*, western blot analysis of protein expression and phosphorylation levels of LATS, YAP, and TAZ in SKOV3 cells cultured in 2D or 3D (with gellan gum) with DMSO or GA-017. β-Actin was used for an internal control. The data are representative of three independent experiments. *D*, dose-response to GA-017 for 1 h. *E*, time course response to 10 μM GA-017. *F–H*, nuclear translocation of YAP in SKOV3 cells cultured in 2D with DMSO or GA-017, detected by immunofluorescent staining. The data represent means ± SD of three independent experiments. *F*, fluorescent images of YAP nuclear translocation after treatment with 10 μM GA-017 for 4 h. The data are representative of three

(Figs. 3*E* and S3, *E* and *G* and Table S6).The decrease of LATS proteins appeared a secondary effect, as it was seen 6 to 24 h after the GA-017 treatment, which contrasts with the immediate decrease of phosphorylated YAP/TAZ in 1 h (Figs. 3*E* and S3*G* and Table S6). We observed that MG-132, a proteasome inhibitor, restored the decrease of LATS proteins by GA-017 (Fig. S3*H* and Table S6), suggesting the LATS degradation *via* the ubiquitin-proteasome system (14). However, the detailed mechanism of LATS degradation by GA-017 remains to be elucidated.

We next evaluated the effect of GA-017 on the nuclear translocation of YAP/TAZ. Consistent with the previous results highlighting the decreased phosphorylation of YAP, GA-017–treated cells exhibited a marked localization of YAP in the nucleus, apparent in data provided by immunofluorescence microscopy (Figs. 3*F* and S4, *C* and *D*). GA-017 enhanced YAP nuclear translocation more efficiently at high cell density (>90% confluence) than at low cell density (<20% confluence) (Fig. S4, *C* and *D*). Subcellular fractionation analysis also revealed a time- and dose-dependent YAP nuclear translocation in cells treated with GA-017 (Fig. 3, *G* and *H*). We observed enhanced YAP nuclear translocation by GA-017 in HUVECs and MSCs as well as SKOV3 cells (Fig. S4, *E* and *F*) and a GA-017 dose-dependent decrease in YAP phosphorylation in HUVECs (Fig. S4, *G* and *H*). Western blot analysis similarly showed that GA-017 increased YAP nuclear translocation (Fig. S4*I*). GA-017 also enhanced the nuclear translocation of TAZ in a time-dependent manner (Fig. 3*I*). In addition, Verteporfin (19), a potent inhibitor of the interaction of YAP/TAZ with transcriptional-enhanced associate domains, abolished the growth-promoting effect of GA-017 (Fig. 3*J*). Verteporfin also inhibited GA-017–mediated induction of *ANKRD1*, *CYR61* and *CTGF*, YAP/TAZ-regulated genes in SKOV3 cells (Figs. 3*K* and S3*I*). Furthermore, Verteporfin suppressed the inhibitory effect of GA-017 on apoptosis induction in HUVECs under 3D conditions (Fig. S5, *A* and *B*). Fig. S5*C* also showed that Verteporfin inhibited GA-017–mediated induction of *ANKRD1*. In addition, we confirmed that siRNA-mediated knockdown of YAP/TAZ in HUVECs reduced the cell death-suppressing activity of GA-017 (Fig. S5, *D* and *E*). Collectively, our results suggest that GA-017 inhibits the Hippo pathway to promote YAP/TAZ stabilization and nuclear translocation, which subsequently leads to enhanced cell growth under 3D cell culture conditions.

GA-017 inhibits LATS1/2 in a manner involving ATP-binding competition

To determine the molecular mechanism of GA-017–induced inhibition of YAP/TAZ phosphorylation, we first profiled the inhibitory effect of GA-017 at a concentration of 100 nM against a panel of 321 diverse kinases. GA-017 inhibited the activity of 16 kinases of the AGC family (20) by more than 65% in this screening (Fig. 4*A* and Table S7). To conduct a more thorough investigation into kinase specificity and select kinases inhibited by GA-017 for further investigation, we evaluated the kinase-inhibitory activity of GA-002, a compound that shares a similar chemical structure to GA-017 and exhibited comparable activity in promoting cell proliferation, spheroid formation, Hippo pathway–regulated gene induction, inhibition of YAP/TAZ phosphorylation, and induction of YAP nuclear translocation (Fig. S6, *A*–*F* and Table S6). Among the 16 kinases, both GA-002 and GA-017 inhibited LATS2, mitogen and stress activated protein kinase 1, ribosomal protein S6 kinase B1 (p70S6K), protein kinase, cAMP-dependent, catalytic, alpha and beta (PKACα and β), and serum/glucocorticoid-regulated kinase 2 and 3 (SGK2 and 3) by more than 65% (Table S7). Subsequently, we determined the 50% inhibition concentration (IC_{50}) values of GA-002 and GA-017 against these seven kinases and found that LATS2 kinase exhibited the greatest degree of attenuation by both GA-002 and GA-017 (Table S7).

Importantly, LATS2 is a core kinase in the Hippo pathway, functioning to phosphorylate YAP/TAZ, thus inhibiting its nuclear translocation (14). Therefore, we investigated the inhibitory activity and manner of both GA-002 and GA-017 against LATS1 and 2 in greater detail. IC_{50} values of GA-017 against LATS1 and 2 were 4.10 ± 0.79 and 3.92 ± 0.42 nM, respectively (Fig. 4, *B* and *C*). A double-reciprocal Lineweaver-Burk plot showed that GA-017 competitively inhibited LATS1 and 2 against ATP, with Ki (inhibition constant) values of 0.58 ± 0.11 and 0.25 ± 0.03 nM, respectively (Fig. 4, *D* and *E*). GA-002, a chemical analog of GA-017, also exhibited comparable inhibition of LATS1 and 2 (Fig. S7, *A*–*C*). These results demonstrate that GA-002 and GA-017 are selective and potent inhibitors of LATS1 and 2, key components in the Hippo pathway, and function by competing with ATP for binding to substrates.

LATS1/2 inhibition is responsible for GA-017–mediated enhanced cell growth

In the kinase assay described above, excluding LATS1/2, GA-017 inhibited the activity of six kinases (mitogen and stress activated protein kinase 1, p70S6K, PKACα, PKACβ, SGK2, and SGK3) at an IC_{50} of <40 nM (Table S7). We then examined whether inhibition of these six kinases would promote cell proliferation under both 2D and 3D conditions, using U-bottom and flat-bottom plates containing gellan gum. We selected eight small-molecule compounds known to inhibit each of these kinases (Table S8) and examined their

independent experiments. *G*, time course response to DMSO or 10 μM GA-017. Y-axis indicates the percent of cells with higher YAP signal intensity in the nucleus than the cytoplasm (C < N). $^{**}p<0.01$, $^{***}p<0.001$. *H*, dose-response to GA-017 for 4 h. $^{**}p<0.01$. *I*, nuclear translocation of TAZ in SKOV3 cells cultured in 2D with DMSO or GA-017. Y-axis indicates the percent of cells with higher TAZ signal intensity in the nucleus than the cytoplasm (C < N). The data represent means ± SD of three independent experiments. $^{*}p<0.05$, $^{**}p<0.01$. *J*, SKOV3 cells were cultured with GA-017 and/or Verteporfin (YAP inhibitor) in low-attachment U-bottom plates for 4 days, and cell number was evaluated using an ATP assay. Y-axis indicates relative cell number (% of control) to nontreatment control (NT). $^{*}p<0.05$. *K*, relative *ANKRD1* mRNA expression in SKOV3 cells treated with DMSO or 10 μM GA-017 for 1 day in the presence or absence of 1 to 20 μM Verteporfin. Y-axis indicates relative mRNA expression to control (DMSO). The data represent means ± SD of 3 to 5 independent experiments. $^{*}p<0.05$, $^{**}p<0.01$. Statistical significance was analyzed using Dunnett's test for *C*, *H*, *J*, and *K* or Student's *t* test for *B*, *G*, and *I*. YAP, Yes-associated protein; DMSO, dimethyl sulfoxide; TAZ, transcriptional coactivator with PDZ-binding motif.

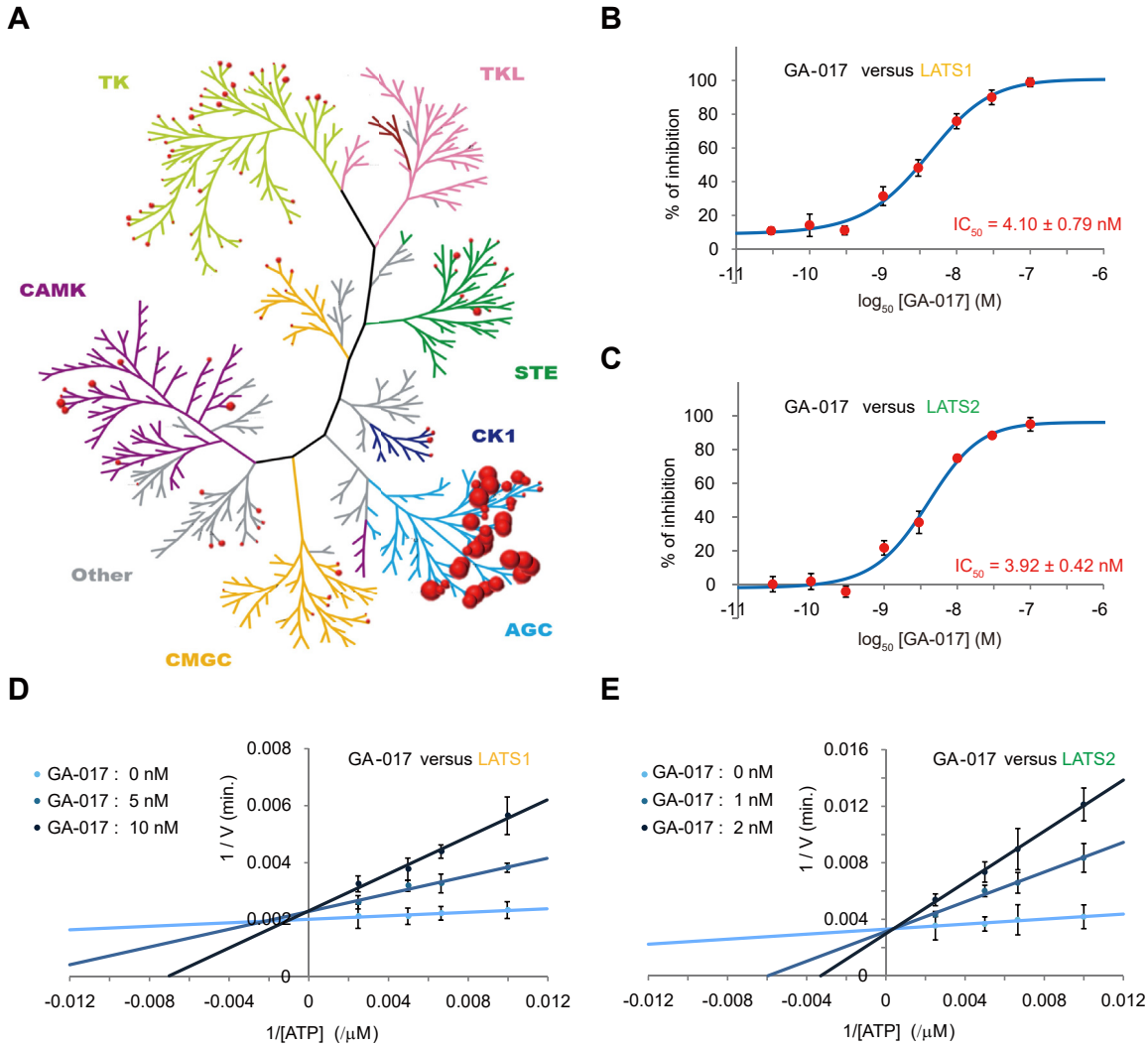

Figure 4. GA-017 inhibits LATS activity. *A*, tree-view map of 321 kinases examined in this study. Kinases inhibited by 0.1 μM GA-017 are indicated by *red circles*, with the size reflecting the degree of inhibition (*i.e.*, with *larger circles* meaning stronger inhibition). Illustration reproduced the courtesy of Carna Biosciences, Inc. *B* and *C*, dose-response curves of GA-017 inhibition rate against LATS1 (*B*) and LATS2 (*C*) in the presence of 400 μM ATP. IC_{50} values were determined based on these experiments. Curve fitting was conducted using ImageJ (version 1.50i, Wayne Rasband National Institutes of Health). The data represent means ± SD of three independent experiments. *D* and *E*, lineweaver-Burk plots (the reciprocal of reaction velocity [V] *versus* reciprocal of the molar concentration of ATP) show the competitive inhibition of ATP by GA-017 against LATS1 (D) and LATS2 (*E*). Reaction velocity was determined as a function of ATP concentration ([ATP]), which was in the range from 100 to 400 μM. The data represent means ± SD of three independent experiments. IC_{50}, 50% inhibition concentration; LATS, large tumor suppressor kinase.

effect on the proliferation of SKOV3 cells under 2D and 3D conditions, in parallel with GA-017. Although 10 μM GA-017 promoted cell growth under 3D conditions, other selected kinase inhibitors did not exhibit growth-promoting effects on SKOV3 cells at any concentration over the range 0.01 to 10 μM (Fig. 5, *A*–*C*). Rather, SB-747651A and AT7867 inhibited the proliferation of cells at a concentration of 10 μM under 3D conditions with gellan gum (Fig. 5*C*). Furthermore, selected kinase inhibitors did not significantly alter the growth-promoting effect of GA-017 (Fig. 5*D*). These results suggest that the inhibitory activity of GA-017 against the six kinases is unlikely responsible for the growth-promoting effect of GA-017.

Next, we deleted the genes encoding LATS1/2 in SKOV3 cells using CRISPR/Cas9 technology to investigate the function of LATS for cell growth under 3D conditions. Immunoblot analysis using antibodies against each of the kinases confirmed that KO cells did not produce LATS1/2 proteins (Fig. 5*E*). We then observed that deletion of the *LATS1* or *LATS2* gene induced an increase in cell proliferation under 3D conditions (Fig. 5*F*). In addition, GA-017 did not exhibit a growth-promoting effect on these mutant cells (Fig. 5*F*). Consistently, deletion of the *LATS1* or *LATS2* gene suppressed the GA-017–mediated induction of *CTGF* mRNA expression (Fig. S3*J*).

We subsequently investigated whether GA-017 affects cell signaling pathways that are independent of YAP/TAZ. It has been reported that LATS1 and/or 2 binds to estrogen receptor-α (ERα), sterol regulatory element-binding protein (SREBP), apoptosis-stimulating protein of p53-1, and regulatory-associated protein of mTOR, regulating their signaling pathways (21–24). Real-time quantitative PCR

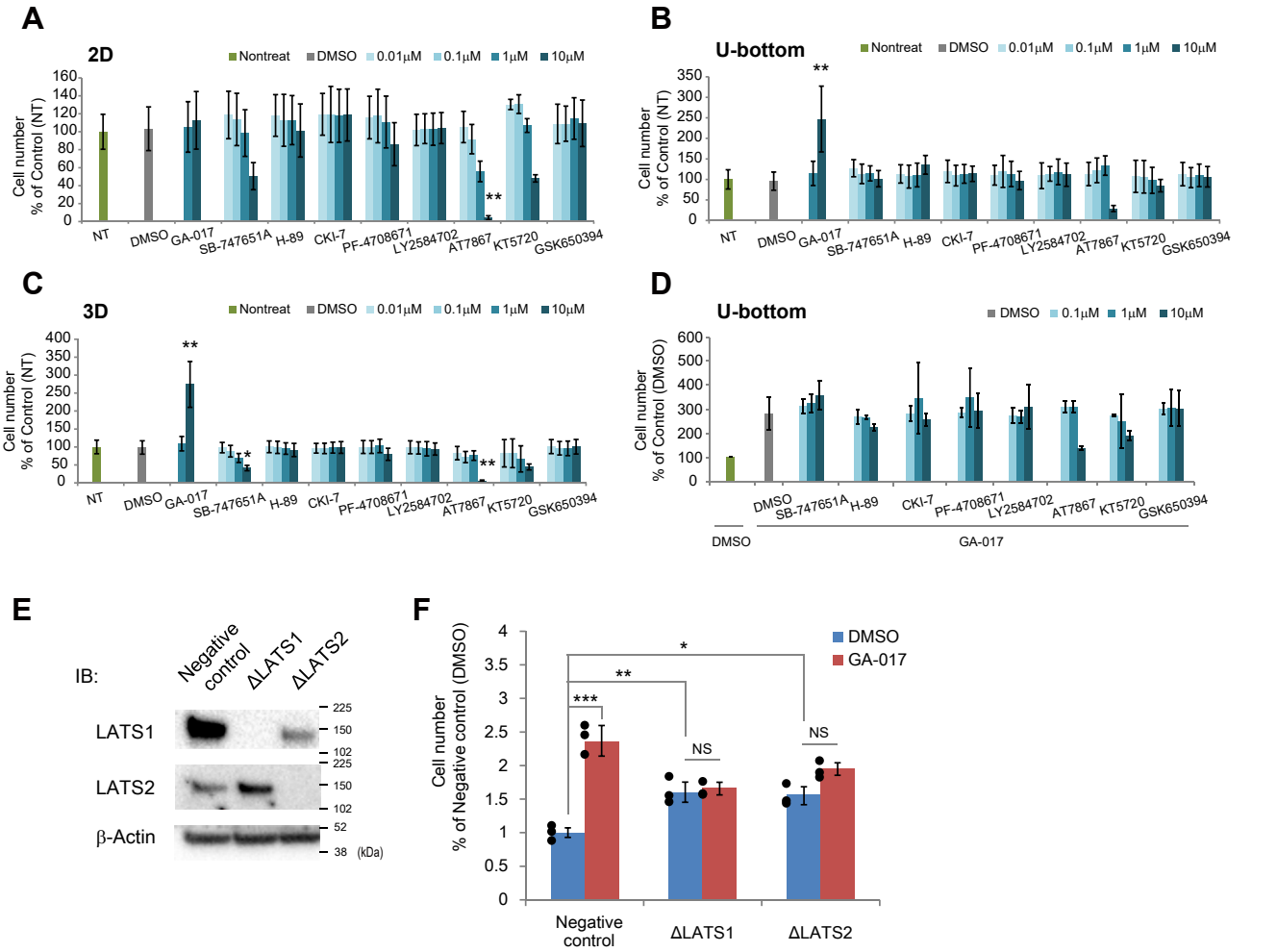

Figure 5. LATS inhibition results in enhanced cell proliferation. *A–C*, SKOV3 cells were cultured for 4 days in normal medium on normal flat-bottom plates (700 cells/well) (*A*) or low-attachment U-bottom plates (700 cells/well) (*B*) or in medium containing gellan gum on low-attachment *flat-bottom plates* (2000 cells/well) (C). DMSO, GA-017, or indicated kinase inhibitors were added during the culture. Cell number was evaluated using an ATP assay. Y-axis indicates relative cell number (% of control) to nontreatment control (NT). The data represent means ± SD of three independent experiments. Statistical significance was analyzed using Dunnett's test. *D*, SKOV3 cells were cultured for 4 days on low-attachment U-bottom plates with DMSO or 10 μM GA-017 in the presence or absence of 0.1 to 10 μM kinase inhibitors. Cell number was evaluated using an ATP assay. Y-axis indicates relative cell number (% of control) to nontreatment control (NT) or vehicle control (DMSO). The data represent means ± SD of three independent experiments. Statistical significance was analyzed using Dunnett's test. *E* and *F*, LATS1 or LATS2 was knocked out using the CRISPR/Cas9 method. *E*, confirmation of LATS1/2 deletion by Western blotting. Negative control was treated similarly in the procedure of the CRISPR/Cas9 method, but LATS1/2 was not deleted. β-Actin was used for an internal control. *F*, Cell growth of negative control, LATS1-deleted or LATS2-deleted cells on low-attachment U-bottom plates for 4 days was evaluated using an ATP assay. DMSO or 10 μM GA-017 was added during the culture. Each RLU was normalized by that of negative control. Statistical significance was analyzed using Tukey's test. The data represent means ± SD of three independent experiments. * $p < 0.05$, ** $p < 0.01$, *** $p < 0.001$. DMSO, dimethyl sulfoxide; LATS, large tumor suppressor kinase.

demonstrated that GA-017 did not significantly affect the expression of ERα-, SREBP-, p53-, or mTOR-regulated genes (Fig. 6*A*), suggesting that GA-017 has little effect on these cell signaling pathways. Moreover, activators and inhibitors of the ERα, SREBP, p53, and mTOR signaling pathways did not exhibit growth-promoting effects on SKOV3 cells under 3D conditions (Fig. 6*B*) and did not alter the growth-promoting effect of GA-017 (Fig. 6*C*). These data indicate that the ERα, SREBP, p53, and mTOR signaling pathways are not likely involved in the growth-promoting effect of GA-017.

Taken together, these results suggest that GA-017 promotes cell proliferation under 3D conditions *via* inhibition of LATS1/2. This corresponds with increased nuclear translocation of the Hippo pathway components YAP/TAZ and subsequent induction of the expression of growth-promoting genes (Fig. 7). In addition, these results suggest that GA-017 stimulates the negative feedback loop in the Hippo pathway, although the mechanism of action remains to be investigated in detail.

Discussion

3D cell culture systems are promising technologies to facilitate the efficient discovery of new drugs, tissue engineering, and stem cell culture for regenerative medicine. Our present study has demonstrated that GA-017 is a novel and useful tool for a wide variety of 3D cell culture applications, such as spheroid and organoid expansion. In particular, GA-017 increases the number and size of spheroids of various cell-types in both scaffold-based and anchorage-independent (scaffold-free) 3D cultures. It is worth noting that GA-017

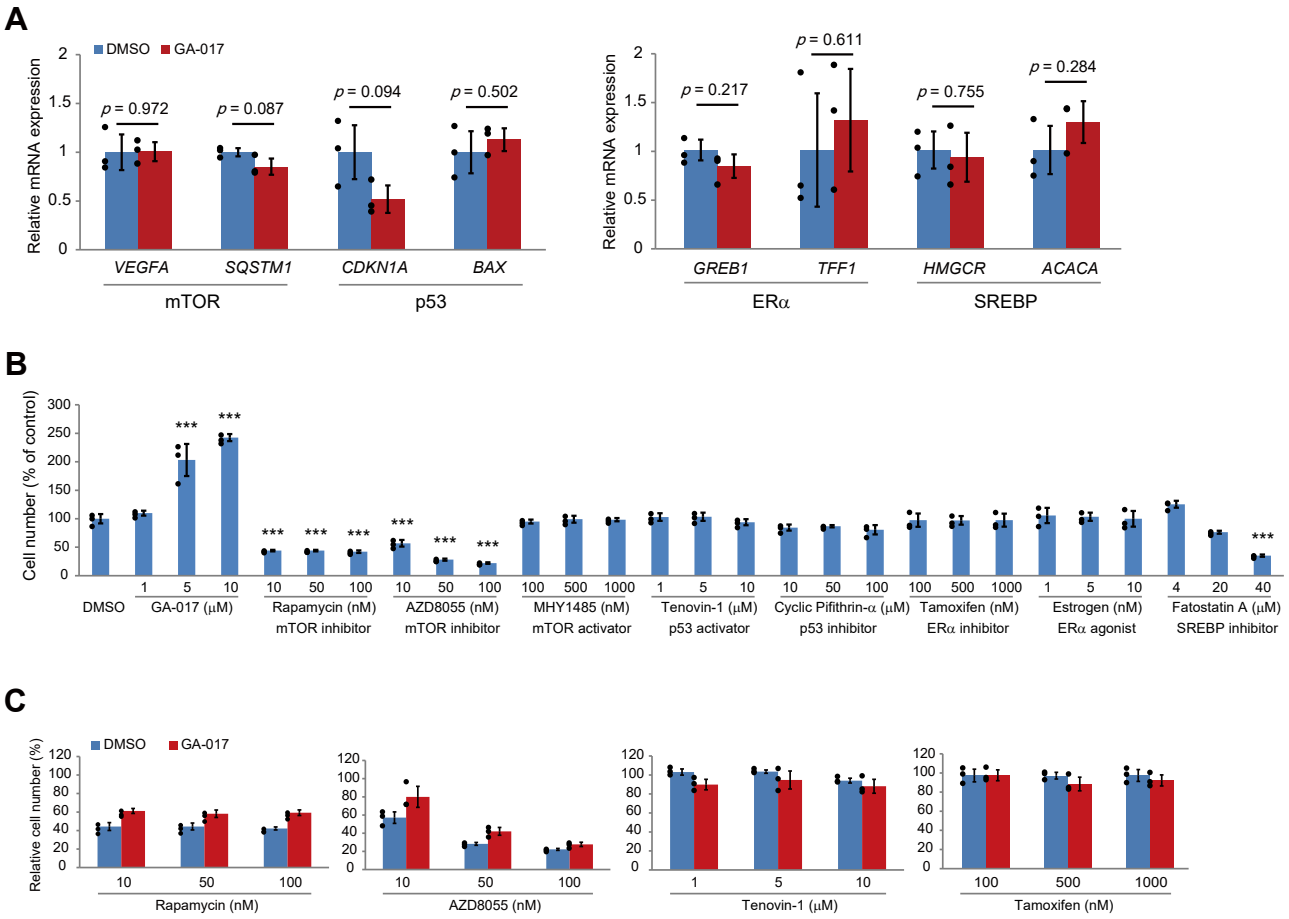

Figure 6. GA-017 does not affect signaling pathways other than YAP/TAZ. *A*, the mRNA expression of ERα-, p53-, mTOR-, and SREBP-regulated genes in SKOV3 cells cultured in medium containing gellan gum with DMSO or 10 μM GA-017 for 1 day. Signals were normalized by that of the *GAPDH* gene. Y-axis indicates relative mRNA expression to vehicle control (DMSO). The data represent means ± SD of three independent experiments. Statistical significance was analyzed using Student's *t* test. *B*, SKOV3 cells were cultured in wells of low-attachment U-bottom plates with DMSO, GA-017, or indicated inhibitors and activators for 4 days. Cell number was evaluated using an ATP assay. Statistical significance was analyzed using Dunnett's test. The data represent means ± SD of three independent experiments. *C*, SKOV3 cells were cultured in the presence of 10 μM GA-017 with DMSO or indicated inhibitors and activators for 4 days. Cell number was evaluated using an ATP assay. The data represent means ± SD of three independent experiments. Statistical significance was analyzed using Student's *t* test. ***$p < 0.001$.; DMSO, dimethyl sulfoxide; ERα, estrogen receptor-α; SREBP, sterol regulatory element-binding protein; TAZ, transcriptional coactivator with PDZ-binding motif; YAP, Yes-associated protein.

induces the growth of cells that lose their proliferative capacity under anchorage-independent conditions, for instance, HUVECs and MSCs; therefore, GA-017 is useful for expanding colonies of such limited resources. Although our data revealed that GA-017 has little effect on the expression of their molecular markers during culture, further research will be necessary to implement detailed characterization of GA-017–expanded cells. Furthermore, we have proven that GA-017 is a selective and potent small molecule inhibitor of LATS1/2, which serves as a major component of the Hippo pathway. Inhibition of the Hippo pathway mediated by GA-017 is consistent with the accelerated growth of cells treated with this chemical. GA-017 will also be a valuable agent to investigate the mechanism of Hippo pathway–mediated cellular functions, including proliferation, apoptosis, differentiation, and self-renewal.

The core Hippo pathway transduces signals from the cell membrane into the nucleus, where the upstream kinases, MST1 and MST2 (17), phosphorylate and activate LATS1/2. Once activated, LATS1/2 phosphorylates the transcriptional coactivators, YAP/TAZ, sequentially promoting their nuclear exclusion and/or cytoplasmic degradation. Our data revealed that GA-017 inhibits LATS1/2, thereby enhancing the accumulation of YAP/TAZ in the nucleus, which in turn induces the expression of Hippo pathway–related genes such as *ANKRD1*, *CYR61*, and *CTGF*. During anchorage-independent culture, cells in spheroids are at a high density and shaped round, detecting increased cell–cell contact. Under this mechanical stress condition, YAP/TAZ becomes highly phosphorylated and is exported out of the nucleus (25, 26). The growth-promoting effect of GA-017 under 3D culture conditions could be attributed to the inhibition of YAP/TAZ phosphorylation resulting from increased cell–cell contact. Consistently, it has been reported that LATS1/2 deletion strongly increases anchorage-independent growth in many cancer cell lines (27, 28). A similar result was obtained in cells that overexpress microRNA-372, which directly targets LATS2 (29). LATS1/2 activators such as MOB1A/1B (30) and

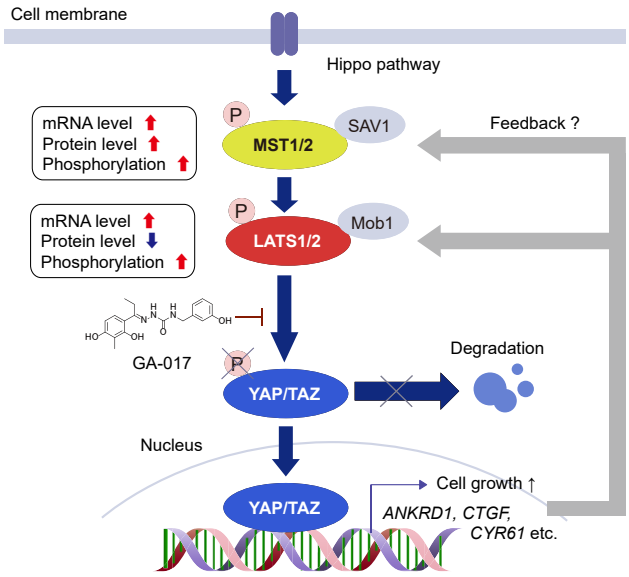

Figure 7. Proposed mechanism of action of GA-017. GA-017 inhibits the kinase activity of LATS1/2 and subsequently stabilizes YAP/TAZ, inducing the expression of YAP/TAZ-regulated genes. The gene products consequently enhance the proliferation of cells. Subsequently observed changes in MST1/2 and LATS1/2 are indicated on the *left*. A possible feedback is also shown. LATS, large tumor suppressor protein; MST, Mammalian Ste20-like kinase; TAZ, transcriptional coactivator with PDZ-binding motif; YAP, Yes-associated protein.

Angiomotins (31) are identically the target of genetic deletion to attain YAP/TAZ activation. These results indicate that the suppression of LATS expression or function by genetic manipulation is also a valid approach to accelerate spheroid and organoid expansion. Moreover, GA-017 will be useful in cell expansion with the great advantage of being able to control LATS function for a desired length of time, simply by adding it to the culture medium.

Small molecule inhibitors of LATS1/2 offer the potential of playing a crucial role in drug discovery. The use of 3D cell culture models in the drug screening process is expected to yield a more accurate therapeutic prediction for clinical outcomes. However, the application of 3D cell culture in HTS remains a challenge, due to difficulties in preparing a sufficient number of spheroids or organoids. For example, there have been many attempts to construct HTS-compatible culture systems for patient-derived cancer spheroids and organoids (32, 33). GA-017 may be beneficial in improving the efficiency of tumor-derived organoid and spheroid preparation and permit expansion, yielding large quantities. The ability of GA-017 to enhance the growth of cells derived from a dynamic range of tissues is advantageous for this purpose. It remains unclear, however, why GA-017 fails to exhibit growth-promoting effects in HepG2 and LNCap cell lines.

Organoid technology holds remarkable potential for not only basic research and drug discovery but also clinical application. Recent studies have indicated that organoids are applicable to transplantation therapy in mouse models, employing these techniques to treat intestine, colon, liver, pancreatic islet, and kidney injury (10, 34, 35). YAP/TAZ are essential for the maintenance of stemness and self-renewal properties of intestinal, mammary, pancreatic, and airway organoids (36–38). Our data indicated that GA-017 enhances the growth of intestinal organoids. Although further detailed investigation is needed, GA-017 may function as a general tool for expanding other types of organoids *ex vivo*.

Another potential application of small-molecule LATS1/2 inhibitors such as GA-017 is the development of therapeutic drugs. Recent studies have extended the potential uses of YAP/TAZ for tissue repair and regenerative medicine. In mouse liver injury models, YAP is activated after partial hepatectomy, whereas deletion of YAP/TAZ resulted in a delay of liver regeneration (39). Similar changes in the YAP activity have been reported in studies of the heart, skin, and muscle (40–42). Furthermore, YAP is associated with the onset of Alzheimer's disease (43). These studies suggest that pharmacological modulation of the Hippo pathway would be beneficial in presenting potential therapeutic cures of organ injury and damage.

In agreement with the importance of the Hippo pathway in pharmaceutical medicine, several small-molecule modulators of the Hippo pathway have been identified as organ-regenerative reagents. The selective MST1/2 inhibitor, XMU-MP-1, promotes tissue repair and regeneration in murine models of liver and intestine injury (44). Neratinib improves pancreatic beta-cell function and survival by inhibiting MST1 in diabetic mouse models (45). The TAZ activator, IBS008738, facilitates muscle repair in a mouse injury model (46). In line with these approaches, it will be interesting to test the efficiency of GA-017 to promote tissue repair in mouse injury models. However, GA-017 shows incomplete selectivity for LATS1/2 over other kinases in the AGC family. Therefore, further structural optimization, utilizing technologies in medicinal chemistry may be necessary to obtain more potent and selective LATS1/2 inhibitors.

Conversely, there is some concern about pharmaceutical YAP/TAZ activation for regenerative medicine. For instance, sustained activation of YAP/TAZ can lead to organ overgrowth and tumorigenesis (47). Despite this adverse effect, organ overgrowth caused by transient YAP overproduction has been reported to be reversible upon cessation of its activation (48). Several reports suggested that activation of YAP/TAZ alone is not sufficient to elicit cancer development (49, 50). In addition, deletion of LATS1/2 in cancer cell lines inhibits tumor growth in murine models (27). Nevertheless, the administration period of YAP/TAZ modulators must be cautiously controlled to avoid the risk of tumor formation.

In conclusion, we identified a novel small molecule, GA-017, as an activator of cell proliferation by conducting 3D culture–oriented HTS. Moreover, we found that potent LATS1/2 inhibition by GA-017, which subsequently activates YAP/TAZ, promotes cell growth under 3D culture conditions. To the best of our knowledge, GA-017 is the first LATS1/2 inhibitor that exhibits sufficient growth-promoting effect on a variety of cell types under 3D conditions. Our results will provide valuable insights into novel drug screening systems, cell therapies employing spheroids/organoids, and pharmacological organ regeneration.

Experimental procedures

Chemical compounds

GA-002 [(E)-N'-(1-(2,4-dihydroxy-3-methylphenyl)propylidene)-2-(phenylamino)propanehydrazide] and GA-017 [(E)-2-(1-(2,4-dihydroxy-3-methylphenyl)propylidene)-N-(3-hydroxybenzyl)hydrazine-1-carboxamide] were prepared using standard synthetic procedures as described in the Supporting information.

Reagents

Gellan gum (Kelcogel CG-LA) was purchased from Sansho. All the small molecule chemicals including GA-002 and GA-017 as described in the Supporting information were dissolved in DMSO and stocked at −20 °C.

Cells

All cells and media used in this study are summarized in the Supporting information. Cells were cultured at 37 °C in a humidified atmosphere with 5% CO_2.

Mice

C57BL/6N mice were purchased from Charles River Laboratories Japan, Inc. To rule out any influence of distinct commensal bacteria, all mice were housed in the same cage for at least 3 weeks after weaning. These mice were maintained under conventional conditions at Nissan Chemical Corporation. Protocols approved by Nissan Chemical Corporation were used for all animal experiments.

Cell culture using medium with gellan gum

3D suspension cell cultures using gellan gum were previously reported (7). The cells were seeded in a medium containing 0.015% (w/v) of gellan gum and dispensed into the wells of 96-well flat-bottom low-attachment plates (Corning Incorporated) at 2000 cells/well. For the monolayer culture method (2D control), the cells were inoculated in the medium without gellan gum and dispensed into 96-well flat-bottom cell-attachable plates (Corning Incorporated) at 700 cells/well.

HTS using gellan gum

SKOV3 cells were seeded into McCoy's 5A medium containing 100 ng/ml of HB-EGF (PeproTech), 15% (v/v) FBS, and 0.015% (w/v) gellan gum and dispensed into the wells of 384-well flat-bottom low-attachment plates (Corning Incorporated) at 1000 cells/45 μl/well. After incubation at 37 °C for 24 h, 5 μl of medium containing a 10-fold concentration of each chemical compound was added to the above cell culture. The plates were then incubated for 4 days at 37 °C, and the number of cells was determined using the WST-8 assay (51).

Cell proliferation assay

To evaluate cell proliferation, the WST-8 assay, the ATP assay, the trypan blue exclusion assay, and acridine orange and 4′,6-diamidino-2-phenylindole staining assay were used as described in the Supporting information.

Spheroid culture on U-bottom microplates

Cells were seeded in the appropriate medium and dispensed in the wells of 96-well U-bottom low-attachment plates (Corning Incorporated) at 700 cells/90 μl/well. For the drug test, 10 μl of the medium containing a 10-fold concentration of GA-017 was added to the above cell culture. These plates were incubated for 2 to 6 days at 37 °C, and the number of cells was evaluated by the ATP assay.

Hanging drop cell culture

A431 cells were seeded in the indicated medium at a density of 50,000 cells/ml, and 10 μM of GA-017 or DMSO was added to the cell suspension. The cell suspension was seeded by 10 μl in 15 drops on the back surface of the lid of a 3.5-cm dish (Corning Incorporated) to form droplets. The lid was returned to the dish and 2 ml of PBS was added and cultured for 2 days at 37 °C. The cultured droplets were collected and the cell number was counted by the ATP assay.

Cyst culture

Cold Matrigel Matrix GFR (Corning Incorporated) was spread on a 24-well plate at 50 μl per well and allowed to sit at 37 °C for 15 min. MDCK cell suspension (1.1×10^4 cells/ml) in the indicated medium including 0.2% Matrigel Matrix GFR was dispensed to the wells at 900 μl/well. A total of 100 μl of medium containing 100 μM GA-017 or DMSO (0.1%) was then added to the above cell suspension (900 μl), and the plates were incubated for 6 days at 37 °C. The diameter of formed cysts and the population were measured using a Cell^{3}iMager duos (SCREEN Holdings).

Organoid culture

Intestinal organoids were prepared and cultured following the protocol of STEMCELL Technologies Inc., as described in detail in the Supporting information. The number and diameter of the formed intestinal organoids were determined using a Cell^{3}iMager duos (SCREEN Holdings) every 2 or 3 days.

Microarray analysis

Total RNA was isolated from the cells or organoids using an RNeasy Kit (Qiagen) according to the manufacturer's protocol. Each RNA sample was analyzed using a GeneChip Human Gene 2.0ST Array (Affimetrix and KURABO). Genes up- and down-regulated in expression by at least 2-fold were selected using DNA MicroArray Viewer Software (KURABO). All the data are minimum information about a microarray experiment compliant, and the raw data were deposited in the National Center for Biotechnology Information Gene Expression Omnibus under accession number GSE145538.

Real-time PCR

Real-time PCR was carried out for 40 to 45 cycles of 15 s at 95 °C and 1 min at 60 °C using an ABI PRISM 7700 Sequence Detector (Thermo Fisher Scientific). All Taqman primers and probes are described in the Supporting information.

ASBMB

Western blotting

SKOV3 cells were seeded in a medium supplemented with (3D) or without (2D) 0.015% gellan gum and treated with GA-017 or DMSO for the indicated time. Cells were then lysed with RIPA buffer containing Halt Protease and Phosphatase Inhibitors (Thermo Fisher Scientific). Samples were separated by SDS-PAGE, and the proteins in the gel were electrophoretically transferred onto a PVDF membrane (Bio-Rad). The blot was then blocked and incubated with antibodies described in the Supporting information. Next, the blot was incubated with peroxidase-conjugated anti-immunoglobulin (SouthernBiotech). Sites of antibody binding were visualized using the ECL Western blotting detection system (FUJIFILM Wako Pure Chemical Corporation, #295-72404) and were subjected to densitometry analysis using ImageJ (version 1.50i, Wayne Rasband National Institutes of Health) and normalized to β-Actin expression.

Nuclear translocation assay

SKOV3 cells were cultured on 96-well cyclo olefin polymer plates (PerkinElmer). The cells treated with GA-002, GA-017, or DMSO were fixed with 4% paraformaldehyde in PBS. The cells were then blocked and incubated with the indicated antibodies, Hoechst33342 (Thermo Fisher Scientific), and secondary antibody. Fluorescent images were analyzed automatically using an Operetta CLS (PerkinElmer) or manually using a confocal fluorescence microscope FV1200 IX83 (Olympus Corporation). The algorithm in Operetta CLS was used to detect the outline of cells and the cell nuclei. The ratio of signal intensity in the nucleus/signal intensity in the cytoplasm was then calculated; 2200 to 2700 cells were analyzed in each experiment. When the ratio (nucleus/cytoplasm) of YAP and TAZ signal intensity was higher than 1.4 and 1.22, respectively, YAP and TAZ were defined as being nuclear translocated. The antibodies are described in the Supporting information.

Kinase panel assay

Kinase inhibitory profiling of GA-002 and GA-017 was conducted at 0.1 μM using an IMAP Assay or Off-chip Mobility-Shift Assay (Carna Biosciences) as described in the Supporting information.

Kinase assay

The kinase assay was performed in 384-well black plates (Greiner Bio-One, #784900) using a Fluorospark Kinase/ADP Multi-Assay kit (FUJIFILM Wako Pure Chemical Corporation) according to manufacturer's protocol at a final volume of 5 μl/well. The details are described further in the Supporting information.

Genome editing

LATS1/2-deficient cells were created using the CRISPR/Cas9 system. SKOV3 cells were transiently transfected with a Cas9 expression plasmid encoding puromycin resistance (Horizon Discovery, U-005100-120) and the complex with crRNA and tracrRNA (Horizon Discovery, U-002005-20). The target sequences of crRNA were 5′- GTGGGCATGAAATCC CTACA-3′ for human LATS1 (Horizon Discovery, CM-003865-01-0002) and 5′-TAGGGTCTTCATGGCGTA CA-3′ for human LATS2 (Horizon Discovery, CM-004632-01-0002). After transient selection with puromycin (3 μg/ml) for 1 week, KO single clones were selected by immunoblot analysis for the lack of LATS1/2 proteins.

Statistical analysis of experimental data

All results are presented as the mean ± SD. Statistical significance was analyzed with Student's *t* test, Tukey's test, or Dunnett's test as indicated in each legend, using EXSAS ver. 7.1.6.1 (Arm Systex). The level of significance was set at 0.05 unless stated otherwise.

Data availability

All the data are included in the article. All unique reagents generated in this study are available from the corresponding authors with a completed Materials Transfer Agreement.

Supporting information—This article contains the supporting information (52–61).

Acknowledgments—We thank H. Hoshino and H. Konari for technical assistance and Dr A. Iwama and Dr N. Itasaki for reading the article. This work was supported by Nissan Chemical Corporation.

Author contributions—A. A. and T. N. conceptualization; A. A. and T. N. methodology; A. A., T. I., N. A.-F., K. O., K. S., and T. M. investigation; A. A., T. I., N. A.-F., and T. N., formal analysis; A. A., T. I., N. A.-F., and T. N., writing–original draft.

Conflict of interest—All authors are inventors on patents related to this work. The authors declare that they have no other conflicts of interest with the contents of this article.

Abbreviations—The abbreviations used are: DMSO, dimethyl sulfoxide; ECM, extracellular matrix; ERα, estrogen receptor-α; HTS, high throughput screening; HUVEC, human umbilical vein endothelial cells; IC50, 50% inhibition concentration; LATS, large tumor suppressor kinase; MDCK, Madin-Darby canine kidney; MSCs, mesenchymal stem cells; MST, Mammalian Ste20-like kinase; SREBP, sterol regulatory element-binding protein; TAZ, transcriptional coactivator with PDZ-binding motif; YAP, Yes-associated protein.

References

1. MacKee, C., and Chaudhry, G. R. (2017) Advances and challenges in stem cell culture. *Colloids Surf. B Biointerfaces* **159**, 62–77
2. Nava, M. M., Raimondi, M. T., and Pietrabissa, R. (2012) Controlling self-renewal and differentiation of stem cells *via* mechanical cues. *J. Biomed. Biotechnol.* **2012**, 797410
3. Fang, Y., and Eglen, R. M. (2017) Three-dimensional cell cultures in drug discovery and development. *SLAS Discov.* **22**, 456–472
4. Kapałczyńska, M., Kolenda, T., Przybyła, W., Zajączkowska, M., Teresiak, A., Filas, V., Ibbs, M., Bliźniak, R., Łuczewski, Ł., and Lamperska, K.

(2018) 2D and 3D Cell Cultures - a comparison of different types of cancer cell cultures. *Arch. Med. Sci.* **14**, 910–919
5. Pampaloni, F., Reynaud, E. G., and Stelzer, E. H. (2007) The third dimension bridges the gap between cell culture and live tissue. *Nat. Rev. Mol. Cell. Biol.* **8**, 839–845
6. Breslin, S., and O'Driscoll, L. (2013) Three-dimensional cell culture: The missing link in drug discovery. *Drug Discov. Today* **18**, 240–249
7. Aihara, A., Abe, N., Saruhashi, K., Kanaki, T., and Nishino, T. (2016) Novel 3-D cell culture system for *in vitro* evaluation of anticancer drugs under anchorage-independent conditions. *Cancer Sci.* **107**, 1858–1866
8. Lancaster, M. A., and Knoblich, J. A. (2014) Organogenesis in a dish: Modeling development and disease using organoid technologies. *Science* **345**, 1247125
9. Brassard, J. A., and Lutolf, M. P. (2019) Engineering stem cell self-organization to build better organoids. *Cell Stem Cell* **24**, 860–876
10. Xu, H., Jiao, Y., Qin, S., Zhao, W., Chu, Q., and Wu, K. (2018) Organoid technology in disease modelling, drug development, personalized treatment and regeneration medicine. *Exp. Hematol. Oncol.* **7**, 30
11. Edmondson, R., Broglie, J. J., Adcock, A. F., and Yang, L. (2014) Three-dimensional cell culture systems and their applications in drug discovery and cell-based biosensors. *Assay Drug Dev. Technol.* **12**, 207–218
12. Hong, W., and Guan, K. L. (2012) The YAP and TAZ transcription coactivators: Key downstream effectors of the mammalian Hippo pathway. *Semin. Cell Dev. Biol.* **23**, 785–793
13. Totaro, A., Panciera, T., and Piccolo, S. (2018) YAP/TAZ upstream signals and downstream responses. *Nat. Cell Biol.* **20**, 888–899
14. Furth, N., and Aylon, Y. (2017) The LATS1 and LATS2 tumor suppressors: Beyond the Hippo pathway. *Cell. Death Differ.* **24**, 1488–1501
15. Meng, Z., Moroishi, T., and Guan, K. L. (2016) Mechanisms of Hippo pathway regulation. *Gene Dev.* **30**, 1–17
16. Ma, S., Meng, Z., Chen, R., and Guan, K. L. (2019) The Hippo pathway: Biology and pathophysiology. *Annu. Rev. Biochem.* **88**, 577–604
17. Thompson, B. J., and Sahai, E. (2015) MST kinases in development and disease. *J. Cell Biol.* **210**, 871–882
18. Moroishi, T., Park, H. W., Qin, B., Chen, Q., Meng, Z., Plouffe, S. W., Taniguchi, K., Yu, F. X., Karin, M., Pan, D., and Guan, K. L. (2015) A YAP/TAZ-induced feedback mechanism regulates Hippo pathway homeostasis. *Genes Dev.* **29**, 1271–1284
19. Liu-Chittenden, Y., Huang, B., Shim, J. S., Chen, Q., Lee, S., Anders, R. A., Liu, J. O., and Pan, D. (2012) Genetic and pharmacological disruption of the TEAD-YAP complex suppresses the oncogenic activity of YAP. *Genes Dev.* **26**, 1300–1305
20. Leroux, A. E., Schulze, J. O., and Biondi, R. M. (2018) AGC kinases, mechanisms of regulation and innovative drug development. *Semin. Cancer Biol.* **48**, 1–17
21. Britschgi, A., Duss, S., Kim, S., Couto, J. P., Brinkhaus, H., Koren, S., De Silva, D., Mertz, K. D., Kaup, D., Varga, Z., Voshol, H., Vissieres, A., Leroy, C., Roloff, T., Stadler, M. B., *et al.* (2017) The Hippo kinases LATS1 and 2 control human breast cell fate *via* crosstalk with ERα. *Nature* **541**, 541–545
22. Aylon, Y., Gershoni, A., Rotkopf, R., Biton, I. E., Porat, Z., Koh, A. P., Sun, X., Lee, Y., Fiel, M.-I., Hoshida, Y., Friedman, S. L., Johnson, R. L., and Oren, M. (2016) The LATS2 tumor suppressor inhibits SREBP and suppresses hepatic cholesterol accumulation. *Genes Dev.* **30**, 786–797
23. Ofir-Rosenfeld, Y., A, Y., Yabuta, N., Lapi, E., Nojima, H., Lu, X., and Oren, M. (2010) The Lats2 tumor suppressor augments p53-mediated apoptosis by promoting the nuclear proapoptotic function of ASPP1. *Genes Dev.* **24**, 2420–2429
24. Gan, W., Dai, X., Dai, X., Xie, J., Yin, S., Zhu, J., Wang, C., Liu, Y., Guo, J., Wang, M., Liu, J., Hu, J., Quinton, R. J., Ganem, N. J., Liu, P., *et al.* (2020) LATS suppresses mTORC1 activity to directly coordinate Hippo and mTORC1 pathways in growth control. *Nat. Cell Biol.* **22**, 246–256
25. Panciera, T., Azzolin, L., Cordenonsi, M., and Piccolo, S. (2017) Mechanobiology of YAP and TAZ in physiology and disease. *Nat. Rev. Mol. Cell Biol.* **18**, 758–770
26. Dasgupta, I., and McCollum, D. (2019) Control of cellular responses to mechanical cues through YAP/TAZ regulation. *J. Biol. Chem.* **294**, 17693–17706
27. Moroishi, T., Hayashi, T., Pan, W. W., Fujita, Y., Holt, M. V., Qin, J., Carson, D. A., and Guan, K. L. (2016) The Hippo pathway kinases LATS1/2 suppress cancer immunity. *Cell* **167**, 1525–1539
28. Pan, W. W., Moroishi, T., Koo, J. H., and Guan, K. L. (2019) Cell type-dependent function of LATS1/2 in cancer cell growth. *Oncogene* **38**, 2595–2610
29. Cheng, X., Chen, J., and Huang, Z. (2018) miR-372 promotes breast cancer cell proliferation by directly targeting LATS2. *Exp. Ther. Med.* **15**, 2812–2817
30. Nishio, M., Sugimachi, K., Goto, H., Wang, J., Morikawa, T., Miyachi, Y., Takano, Y., Hikasa, H., Itoh, T., Suzuki, S. O., Kurihara, H., Aishima, S., Leask, A., Sasaki, T., Nakano, T., *et al.* (2016) Dysregulated YAP1/TAZ and TGF-β signaling mediate hepatocarcinogenesis in Mob1a/1b-deficient mice. *Proc. Natl. Acad. Sci.U. S. A.* **113**, E71–80
31. Mana-Capelli, S., and McCollum, D. (2018) Angiomotins stimulate LATS kinase autophosphorylation and act as scaffolds that promote Hippo signaling. *J. Biol. Chem.* **293**, 18230–18241
32. Booij, T. H., Price, L. S., and Danen, E. H. J. (2019) 3D cell-based assays for drug screens: Challenges in imaging, image analysis, and high-content analysis. *SLAS Discov.* **24**, 615–627
33. Kondo, J., and Inoue, M. (2019) Application of cancer organoid model for drug screening and personalized therapy. *Cells* **8**, 470
34. Pawitan, J. A. (2018) Advances in regenerative medicine: From stem cells to organoids. *J. Bios. Med.* **6**, 128–136
35. Prior, N., Inacio, P., and Huch, M. (2019) Liver organoids: From basic research to therapeutic applications. *Gut* **68**, 2228–2237
36. Panciera, T., Azzolin, L., Fujimura, A., Biagio, D. D., Frasson, C., Bresolin, S., Soligo, S., Basso, G., Rosato, A., Cordenonsi, M., and Piccolo, S. (2016) Induction of expandable tissue-specific stem/progenitor cells through transient expression of YAP/TAZ. *Cell Stem Cell* **19**, 725–737
37. Sachs, N., Papaspyropoulos, A., Ommen, D. D. Z., Heo, I., Böttinger, L., Klay, D., Weeber, F., Huelsz-Prince, G., Iakobachvili, N., Amatngalim, G. D., de Ligt, J., van Hoeck, A., Proost, N., Viveen, M. C., Lyubimova, A., *et al.* (2019) Long-term expanding human airway organoids for disease modeling. *EMBO J.* **38**, e100300
38. Serra, D., Mayr, U., Boni, A., Lukonin, I., Rempfler, M., Meylan, L. C., Stadler, M. B., Strnad, P., Papasaikas, P., Vischi, D., Waldt, A., Roma, G., and Liberali, P. (2019) Self-organization and symmetry breaking in intestinal organoid development. *Nature* **569**, 66–72
39. Lu, L., Finegold, M. J., and Johnson, R. L. (2018) Hippo pathway coactivators Yap and Taz are required to coordinate mammalian liver regeneration. *Exp. Mol. Med.* **50**, e423
40. Lee, M.-J., Byun, M. R., Furutani-Seiki, M., Hong, J.-H., and Jung, H.-S. (2014) YAP and TAZ regulate skin wound healing. *J. Invest. Dermatol.* **134**, 518–525
41. Xin, M., Kim, Y., Sutherland, L. B., Murakami, M., Qi, X., McAnally, J., Porrello, E. R., Mahmoud, A. I., Tan, W., Shelton, J. M., Richardson, J. A., Sadek, H. A., Bassel-Duby, R., and Olson, E. N. (2013) Hippo pathway effector Yap promotes cardiac regeneration. *Proc. Natl. Acad. Sci. U. S. A.* **110**, 13839–13844
42. Watt, K. I., Turner, B. J., Hagg, A., Zhang, X., Davey, J. R., Qian, H., Beyer, C., Winbanks, C. E., Harvey, K. F., and Gregorevic, P. (2015) The Hippo pathway effector YAP is a critical regulator of skeletal muscle fibre size. *Nat. Commun.* **6**, 6048
43. Tanaka, H., Homma, H., Fujita, K., Kondo, K., Yamada, S., Jin, X., Waragai, M., Ohtomo, G., Iwata, A., Tagawa, K., Atsuta, N., Katsuno, M., Tomita, N., Furukawa, K., Saito, Y., *et al.* (2020) YAP-dependent necrosis occurs in early stages of Alzheimer's disease and regulates mouse model pathology. *Nat. Commun.* **11**, 507
44. Fan, F., He, Z., Kong, L.-L., Chen, Q., Yuan, Q., Zhang, S., Ye, J., Liu, H., Sun, X., Geng, J., Yuan, L., Hong, L., Xiao, C., Zhang, W., Sun, X., *et al.* (2016) Pharmacological targeting of kinases MST1 and MST2 augments tissue repair and regeneration. *Sci. Transl. Med.* **8**, 352ra108
45. Ardestani, A., Li, S., Annamalai, K., Lupse, B., Geravandi, S., Dobrowolski, A., Yu, S., Zhu, S., Baguley, T. D., Surakattula, M., Oetjen, J., Hauberg-Lotte, L., Herranz, R., Awal, S., Altenhofen, D., *et al.* (2019) Neratinib protects pancreatic beta cells in diabetes. *Nat. Commun.* **10**, 5015

46. Yang, Z., Nakagawa, K., Sarkar, A., Maruyama, J., Iwasa, H., Bao, Y., Ishigami-Yuasa, M., Ito, S., Kagechika, H., Hata, S., Nishina, H., Abe, S., Kitagawa, M., and Hata, Y. (2014) Screening with a novel cell-based assay for TAZ activators identifies a compound that enhances myogenesis in C2C12 cells and facilitates muscle repair in a muscle injury model. *Mol. Cell. Biol.* **34**, 1607–1621
47. Lu, L., Li, Y., Kim, S. M., Bossuyt, W., Liu, P., Qiu, Q., Wang, Y., Halder, G., Finegold, M. J., Lee, J.-S., and Johnson, R. L. (2010) Hippo signaling is a potent *in vivo* growth and tumor suppressor pathway in the mammalian liver. *Proc. Natl. Acad. Sci.U. S. A.* **107**, 1437–1442
48. Camargo, F. D., Gokhale, S., Johnnidis, J. B., Fu, D., Bell, G. W., Jaenisch, R., and Brummelkamp, T. R. (2007) YAP1 increases organ size and expands undifferentiated progenitor cells. *Curr. Biol.* **17**, 2054–2060
49. Chen, Q., Zhang, N., Gray, R. S., Li, H., Ewald, A. J., Zahnow, C. A., and Pan, D. (2014) A temporal requirement for Hippo signaling in mammary gland differentiation, growth, and tumorigenesis. *Genes Dev.* **28**, 432–437
50. Schlegelmilch, K., Mohseni, M., Kirak, O., Pruszak, J., Rodriguez, J. R., Zhou, D., Kreger, B. T., Vasioukhin, V., Avruch, J., Brummelkamp, T. R., and Camargo, F. D. (2011) Yap1 acts downstream of α-Catenin to control epidermal proliferation. *Cell* **144**, 782–795
51. Ishiyama, M., Miyazono, Y., Sasamoto, K., Ohkura, Y., and Ueno, K. (1997) A highly water-soluble disulfonated tetrazolium salt as a chromogenic indicator for NADH as well as cell viability. *Talanta* **44**, 1299–1305
52. Sum, T.-H., Sum, T. J., Stokes, J. E., Galloway, W. R. J. D., and Spring, D. R. (2015) Divergent and concise total syntheses of dihydrochalcones and 5-deoxyflavones recently isolated from Tacca species and Mimosa diplotricha. *Tetrahedron* **71**, 4557–4564
53. Samal, R.-P., Khedkar, V. M., Pissurlenkar, R. R. S., Bwalya, A. G., Tasdemir, D., Joshi, R. A., Rajamohanan, P. R., Puranik, V. G., and Coutinho, E. C. (2013) Design, synthesis, structural characterization by IR, (1) H, (13) C, (15) N, 2D-NMR, X-ray diffraction and evaluation of a new class of phenylaminoacetic acid benzylidene hydrazines as pfENR inhibitors. *Chem. Biol. Drug Des.* **81**, 715–729
54. Grimshaw, K. M., Hunter, L.-J. K., Yap, T. A., Heaton, S. P., Walton, M. I., Woodhead, S. J., Fazal, L., Reule, M., Davies, T. G., Seavers, L. C., Lock, V., Lyons, J. F., Thompson, N. T., Workman, P., and Garrett, M. D. (2010) AT7867 is a potent and oral inhibitor of AKT and p70 S6 kinase that induces pharmacodynamic changes and inhibits human tumor xenograft growth. *Mol. Cancer Ther.* **9**, 1100–1110
55. Sherk, A. B., Frigo, D. E., Schnackenberg, C. G., Bray, J. D., Laping, N. J., Trizna, W., Hammond, M., Patterson, J. R., Thompson, S. K., Kazmin, D., Norris, J. D., and McDonnell, D. P. (2008) Development of a small molecule serum and glucocorticoid-regulated kinase 1 antagonist and its evaluation as a prostate cancer therapeutic. *Cancer Res.* **68**, 7475–7483
56. Zhang, Y., Wang, Q., Chen, L., and Yang, H.-S. (2015) Inhibition of p70S6K1 activation by Pdcd4 overcomes the resistance to an IGF-1R/IR inhibitor in colon carcinoma cells. *Mol. Cancer Ther.* **14**, 799–809
57. Osakada, F., Jin, Z.-B., Hirami, Y., Ikeda, H., Danjyo, T., Watanabe, K., Sasai, Y., and Takahashi, M. (2009) *In vitro* differentiation of retinal cells from human pluripotent stem cells by small-molecule induction. *J. Cell Sci.* **122**, 3169–3179
58. Lopes, A. P., van Roon, J. A. G., Blokland, S. L. M., Wang, M., Chouri, E., Hartgring, S. A. Y., van der Wurff-Jacobs, K. M. G., Kruize, A. A., Burgering, B. M. T., Rossato, M., Radstake, T. R. D. J., and Hillen, M. R. (2019) MicroRNA-130a contributes to type-2 classical DC-activation in sjögren's syndrome by targeting mitogen- and stress-activated protein kinase-1. *Front. Immunol.* **10**, 1335
59. Naito, K., Kurihara, K., Moteki, H., Kimura, M., Natsume, H., and Ogihara, M. (2019) Effect of selective serotonin (5-HT) 2B receptor agonist BW723C86 on epidermal growth factor/transforming growth factor-α receptor tyrosine kinase and ribosomal p70 S6 kinase activities in primary cultures of adult Rat hepatocytes. *Biol. Pharm. Bull.* **42**, 631–637
60. Gantner, F., Götz, C., Gekeler, V., Schudt, C., Wendel, A., and Hatzelmann, A. (1998) Phosphodiesterase profile of human B lymphocytes from normal and atopic donors and the effects of PDE inhibition on B cell proliferation. *Br. J. Pharmacol.* **123**, 1031–1038
61. Naqvi, S., Macdonald, A., McCoy, C. E., Darragh, J., Reith, A. D., and Arthur, J. S. C. (2012) Characterization of the cellular action of the MSK inhibitor SB-747651A. *Biochem. J.* **441**, 347–357